Recurrent Fuzzy Neural Network Controller Design for Ultrasonic Motor Rotor Angle Control

Tien-Chi Chen
Dept. of Computer and Communication
Kun Shan University
Tainan, Taiwan
e-mail: tchichen@mail.ksu.edu.tw

Tsai-Jiun Ren
Dept. of Information Engineering
Kun Shan University
Tainan, Taiwan
e-mail: cyrusren@mail.ksu.edu.tw

Yi-Wei Lou
Dept. of Electrical Engineering
Kun Shan University
Tainan, Taiwan
e-mail: oalatraszi@msn.com

***Abstract*—The ultrasonic motor (USM) has significant high precision, fast dynamic, simple structure and no electromagnetic interference features that are useful in many industrial, medical, robotic and automotive applications. The USM, however has nonlinear characteristics and dead-zone problems due to increasing temperature and motor drive issues under various operating conditions. To overcome these problems a recurrent fuzzy neural network controller (RFNNC) combined with a compensated controller with adjustable parameters and on line learning algorithm is presented in this paper. The proposed control scheme can take the nonlinearity into account and compensate for the USM dead-zone. The proposed control scheme provides robust performance against parameter variations. The experimental results demonstrate the effectiveness of the proposed USM control scheme.**

Keywords- ultrasonic motor; recurrent fuzzy neural network; compensated controller; adjustable parameters; on line learning algorithm.

I. INTRODUCTION

The USM has many excellent features such as high precision, fast dynamics, simple structure, compactness in size and no electromagnetic interference, which is useful in many industrial, medical and automotive applications [1-4]. However, the USM has nonlinear characteristics and a dead-zone problem due to the large static friction torque appearing at low speed [5]. Hence, it is difficult to design a perfect controller to accurately control the USM at all times.

Conventional PI controllers for common motors have the advantages of simple and easy design, high-stability margin and high-reliability when the controllers are tuned properly [6-7]. However, the PI controller cannot maintain these virtues at all times. The USM has nonlinear speed characteristics which vary with the drive operating conditions. A dynamic controller with adjustable parameters and on line learning algorithms is therefore suggested for nonlinear or uncertain dynamics systems [8-11].

This paper presents a new control scheme for USM rotor angle control, the RFNNC combined with a compensated controller that has adjustable parameters and an on-line learning algorithm to overcome the nonlinear characteristic and dead-zone problem. The RFNNC is effective in handling nonlinear motor characteristic variations due to connecting weight updating in the RFNNC. Furthermore, a compensated controller is presented to compensate the USM dead-zone effect, which deteriorates the dynamic response. The proposed control scheme can take the nonlinearity into account and compensate for the USM dead-zone. Robust performance against parameter variations is obtained by the proposed approach. The usefulness and validity of the proposed control scheme is examined through experimental results. The experimental results reveal that the proposed control scheme maintains good, stable performance under different motion conditions.

II. THE PROPOSED CONTROL SCHEME

Fig. 1 shows the proposed control scheme for the USM combined with the RFNNC and compensated controller that has adjustable parameters and an on-line learning algorithm to overcome the nonlinear characteristic and dead-zone problem, where θ_c the USM rotor angle command, θ_r the USM rotor angle, u_R the RFNNC output control force, u_C the compensated controller output control force and u is the total control force.

A. RFNNC Structure

Fig. 2 shows the RFNNC structure, comprised of an input layer, membership layer, rule layer and output layer.

The RFNNC mathematical model is summarized as follows.

(1) Input layer

The RFNNC inputs are $e = \theta_c - \theta_r$ and $\dot{e}$. The outputs $x_{e,i}^1$ and $x_{\dot{e},i}^1$ can be expressed as:

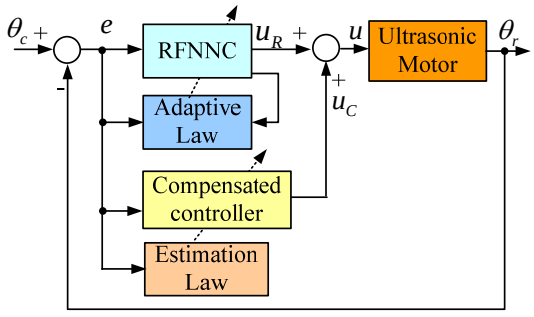

Figure 1. The proposed control scheme for the USM.

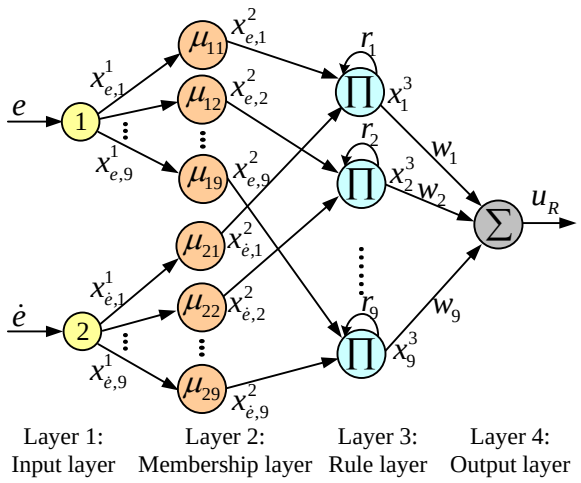

Figure 2. The RFNNC structure.

$$x_{e,i}^1 = e, \quad i = 1,...,9 \tag{1}$$

$$x_{\dot{e},i}^1 = \dot{e}, \quad i = 1,...,9 \tag{2}$$

(2) Membership layer

The membership layer outputs $y_{e,i}^2$ and $y_{\dot{e},i}^2$ can be expressed as a Gaussian function:

$$x_{e,i}^2 = \exp\left(-\left(\frac{x_{e,i}^1 - s_{e,i}}{z_{e,i}}\right)^2\right), \quad i = 1,...,9 \tag{3}$$

$$x_{\dot{e},i}^2 = \exp\left(-\left(\frac{x_{\dot{e},i}^1 - s_{\dot{e},i}}{z_{\dot{e},i}}\right)^2\right), \quad i = 1,...,9 \tag{4}$$

where $\mathbf{S} = \left[s_{e,1},...,s_{e,9},s_{\dot{e},1},...,s_{\dot{e},9}\right]^T$ the mean Gaussian function vector and $\mathbf{Z} = \left[z_{e,1},...,z_{e,9},z_{\dot{e},1},...,z_{\dot{e},9}\right]^T$ is the Gaussian function standard deviation vector.

(3) Rule layer

The rule layer outputs are expressed as:

$$x_i^3(t) = \left(1 + \frac{1}{1+\exp^{-r_i x_i^3(t-1)}}\right) x_{e,i}^2(t) x_{\dot{e},i}^2(t), \quad i = 1,...,9 \tag{5}$$

where $\mathbf{R} = \left[r_1,...,r_9\right]$ is the recurrent weight vector.

(4) Output layer

The output layer outputs u_R can be expressed as:

$$u_R = \sum_{i=1}^{9} w_i x_i^3 = \mathbf{W}^T \mathrm{T}(x,s,z,r) \tag{6}$$

where $\mathbf{T}(x,s,z,r) = \left[x_1^3,...,x_9^3\right]^T$ is fuzzy rule function vector and $\mathbf{W} = \left[w_1,...,w_9\right]^T$ is the adjustable output weight vector.

B. RFNNC and Compensated Controller Design

Consider the USM nonlinear dynamic system is expressed as:

$$\ddot{y} = f(y) + g(y)u(t) + d(t) \tag{7}$$

where $f(y)$ and $g(y)$ are unknown USM functions and assume they are bounded, $u(t)$ the control input, $d(t)$ the external disturbance.

The control goal is to design a RFNNC such that the USM rotor angle tracks the reference model output angle. The tracking error vector is first defined as

$$\mathbf{E} = \left[e,\ \dot{e}\right]^T \tag{8}$$

From (7) and (8), an ideal controller can be chosen as

$$u^*(t) = \frac{1}{g_n(y)}\left[\ddot{y} - f_n(y) - d_n(t) + \mathbf{K}^T\mathbf{E}\right] \tag{9}$$

In (9) , $\mathbf{K} = \left[k_2,\ k_1\right]^T$, in which k_1 and k_2 are positive constants. Applying (7) to (9), the error dynamics can be expressed as

$$\ddot{e} + k_1\dot{e} + k_2 e = 0 \tag{10}$$

If K is chosen to correspond to the coefficients of a Hurwitz polynomial, that is a polynomial whose roots lie strictly in the open left half of the complex plane, then the result achieved where $\lim_{t\to\infty} e(t) = 0$ for any initial conditions. Nevertheless, the functions $f(y)$ and $g(y)$ aren't accurate known and the external load disturbances are perturbed. Thus, the ideal controller $u^*(t)$ cannot be practical implemented. Therefore, the RFNNC will be designed to approximate this ideal controller.

The proposed control scheme for the USM combined by RFNNC and compensated controller is show in Fig. 1. The control force for the USM is the following form:

$$u = u_R + u_C \tag{11}$$

where the RFNNC output control force u_R is the main tracking control to approximate the ideal control force $u^*(t)$. From (7), (9) and (11), an error equation is rewritten as:

$$\dot{\mathbf{E}} = \mathbf{A}\mathbf{E} + \mathbf{B}(u^* - u_R - u_C) \tag{12}$$

where $\mathbf{A} = \begin{bmatrix} 0 & 1 \\ -k_2 & -k_1 \end{bmatrix}$ and $\mathbf{B} = \begin{bmatrix} 0 \\ g(y) \end{bmatrix}$.

Assume that an optimal RFNNC exists to approximate the ideal control force such that

$$u^* = u_R^*(e,\mathbf{W}^*,\mathbf{S}^*,\mathbf{Z}^*,\mathbf{R}^*) + \varepsilon = \mathbf{W}^{*T}\mathbf{T}^* + \varepsilon \tag{13}$$

where ε is a minimum reconstructed error, $\mathbf{W}^*,\mathbf{S}^*,\mathbf{Z}^*,\mathbf{R}^*$ and $\mathbf{T}^*$ are optimal parameters of $\mathbf{W},\mathbf{S},\mathbf{Z},\mathbf{R}$ and $\mathbf{T}$, respectively. Thus, the control force is assumed to take the following form:

$$u = u_R(e,\hat{\mathbf{W}},\hat{\mathbf{S}},\hat{\mathbf{Z}},\hat{\mathbf{R}}) + u_C = \hat{\mathbf{W}}^T\hat{\mathbf{T}} + u_C \tag{14}$$

 ISBN: 978-1-61208-390-2

where $\hat{\mathbf{W}}$, $\hat{\mathbf{S}}$, $\hat{\mathbf{Z}}$, $\hat{\mathbf{R}}$ and $\hat{\mathbf{T}}$ are the optimal parameter estimations provided by tuning the algorithms to be introduced later. Subtracting (14) from (13) an approximation error $\tilde{u}$ is obtained as

$$\begin{aligned}\tilde{u} &= u^* - u = \mathbf{W}^{*T}\mathbf{T}^* + \varepsilon - \hat{\mathbf{W}}^T\hat{\mathbf{T}} - u_C \\ &= \tilde{\mathbf{W}}^T\mathbf{T}^* + \hat{\mathbf{W}}^T\tilde{\mathbf{T}} + \varepsilon - u_C\end{aligned} \tag{15}$$

where $\tilde{\mathbf{W}} = \mathbf{W}^* - \hat{\mathbf{W}}$ and $\tilde{\mathbf{T}} = \mathbf{T}^* - \hat{\mathbf{T}}$. The linearization technique transforms the multidimensional receptive-field basis functions into a partially linear form such that the expansion of $\tilde{\mathbf{T}}$ in Taylor series becomes

$$\tilde{\mathbf{T}} = \left[\tilde{x}_1^3, ..., \tilde{x}_9^3\right]^T = \mathbf{T}_s\tilde{\mathbf{S}} + \mathbf{T}_z\tilde{\mathbf{Z}} + \mathbf{T}_r\tilde{\mathbf{R}} + \mathbf{O}_v \tag{16}$$

where $\tilde{x}_i^3 = x_i^{3*} - \hat{x}_i^3$, x_i^{3*} is the optimal parameter, $\hat{x}_i^3$ is the estimated parameter of x_i^{3*}, $\tilde{\mathbf{S}} = \mathbf{S}^* - \hat{\mathbf{S}}$, $\tilde{\mathbf{Z}} = \mathbf{Z}^* - \hat{\mathbf{Z}}$, $\tilde{\mathbf{R}} = \mathbf{R}^* - \hat{\mathbf{R}}$, $\mathbf{O}_v$ is higher-order terms, $\mathbf{T}_s = \left[\partial x_1^3/\partial s, ..., \partial x_9^3/\partial s\right]_{s=\hat{s}}^T$, $\mathbf{T}_z = \left[\partial x_1^3/\partial z, ..., \partial x_9^3/\partial z\right]_{z=\hat{z}}^T$, $\mathbf{T}_r = \left[\partial y_1^3/\partial r, ..., \partial y_k^3/\partial r\right]_{r=\hat{r}}^T$.

(16) can be rewritten as

$$\mathbf{T}^* = \hat{\mathbf{T}} + \mathbf{T}_s\tilde{\mathbf{S}} + \mathbf{T}_z\tilde{\mathbf{Z}} + \mathbf{T}_r\tilde{\mathbf{R}} + \mathbf{O}_v \tag{17}$$

Substituting (17) into (15), it can be rewritten as:

$$\tilde{u} = \tilde{\mathbf{W}}^T\hat{\mathbf{T}} + \hat{\mathbf{W}}^T(\mathbf{T}_s\tilde{\mathbf{S}} + \mathbf{T}_z\tilde{\mathbf{Z}} + \mathbf{T}_r\tilde{\mathbf{R}}) - u_C + D \tag{18}$$

where $D = \tilde{\mathbf{W}}^T(\mathbf{T}_s\tilde{\mathbf{S}} + \mathbf{T}_z\tilde{\mathbf{Z}} + \mathbf{T}_r\tilde{\mathbf{R}}) + \mathbf{W}^{*T}\mathbf{O}_v + \varepsilon$ is the uncertainty term and this term is assumed to be bounded with a small positive constant β （let $|D| \le \beta$）. From (15) and (18), (12) can be rewritten as

$$\begin{aligned}\dot{\mathbf{E}} &= \mathbf{AE} + \mathbf{B}(u^* - u) = \mathbf{AE} + \mathbf{B}\tilde{u} \\ &= \mathbf{AE} + \mathbf{B}\left[\tilde{\mathbf{W}}^T\hat{\mathbf{T}} + \mathbf{W}\hat{\mathbf{W}}^T(\mathbf{T}_s\tilde{\mathbf{S}} + \mathbf{T}_z\tilde{\mathbf{Z}} + \mathbf{T}_r\tilde{\mathbf{R}}) - u_C + D\right]\end{aligned} \tag{19}$$

Consider the USM dynamic system is represented by (7) if the RFNNC control law is designed as (14) with the adaptive laws for networks parameters, as shown in (20)–(23), and the compensated controller control law is designed as (24) with the estimation law given in (25). The stability of the proposed control scheme can then be guaranteed, where η_1, η_2, η_3, η_4, η_5 are strictly positive constants.

$$\dot{\hat{\mathbf{W}}} = \eta_1\hat{\mathbf{T}}\mathbf{E}^T\mathbf{PB} \tag{20}$$

$$\dot{\hat{\mathbf{S}}} = \eta_2\mathbf{T}_s^T\hat{\mathbf{W}}\mathbf{E}^T\mathbf{PB} \tag{21}$$

$$\dot{\hat{\mathbf{Z}}} = \eta_3\mathbf{T}_z^T\hat{\mathbf{W}}\mathbf{E}^T\mathbf{PB} \tag{22}$$

$$\dot{\hat{\mathbf{R}}} = \eta_4\mathbf{T}_r^T\hat{\mathbf{W}}\mathbf{E}^T\mathbf{PB} \tag{23}$$

$$u_C = \hat{\beta}\,\mathrm{sgn}(\mathbf{E}^T\mathbf{PB}) \tag{24}$$

$$\dot{\hat{\beta}} = \eta_5\left|\mathbf{E}^T\mathbf{PB}\right| \tag{25}$$

Proof: Define a Lyapunov function candidate as

$$\begin{aligned}V(t) = &\frac{1}{2}\mathbf{E}^T\mathbf{PE} + \frac{1}{2\eta_1}tr(\tilde{\mathbf{W}}^T\tilde{\mathbf{W}}) + \frac{1}{2\eta_2}\tilde{\mathbf{S}}^T\tilde{\mathbf{S}} \\ &+ \frac{1}{2\eta_3}\tilde{\mathbf{Z}}^T\tilde{\mathbf{Z}} + \frac{1}{2\eta_4}\tilde{\mathbf{R}}^T\tilde{\mathbf{R}} + \frac{1}{2\eta_5}\tilde{\beta}^2\end{aligned} \tag{26}$$

where $\mathbf{P}$ is a symmetric positive definite matrix which satisfies the following Lyapunov equation

$$\mathbf{A}^T\mathbf{P} + \mathbf{PA} = -\mathbf{Q} \tag{27}$$

where $\mathbf{Q}$ is a positive definite matrix. Here, the uncertainty boundary estimation error is defined as $\tilde{\beta} = \beta - \hat{\beta}$. Taking the Lyapunov function (26) differential and using (18) and (27), it is concluded that

$$\begin{aligned}\dot{V}(t) = &-\frac{1}{2}\mathbf{E}^T\mathbf{QE} + \frac{1}{2}(\mathbf{E}^T\mathbf{PB} + \mathbf{B}^T\mathbf{PE})\tilde{u} - \frac{1}{\eta_1}\tilde{\mathbf{W}}^T\dot{\hat{\mathbf{W}}} \\ &- \frac{1}{\eta_2}\dot{\hat{\mathbf{S}}}^T\tilde{\mathbf{S}} - \frac{1}{\eta_3}\dot{\hat{\mathbf{Z}}}^T\tilde{\mathbf{Z}} - \frac{1}{\eta_4}\dot{\hat{\mathbf{R}}}^T\tilde{\mathbf{R}} - \frac{1}{\eta_5}\tilde{\beta}\dot{\hat{\beta}} \\ = &-\frac{1}{2}\mathbf{E}^T\mathbf{QE} + \mathbf{E}^T\mathbf{PB}\left[\tilde{\mathbf{W}}^T\hat{\mathbf{T}} + \hat{\mathbf{W}}^T(\mathbf{T}_s\tilde{\mathbf{S}} + \mathbf{T}_z\tilde{\mathbf{Z}} + \mathbf{T}_r\tilde{\mathbf{R}}) - u_C + D\right] \\ &- \frac{1}{\eta_1}\tilde{\mathbf{W}}^T\dot{\hat{\mathbf{W}}} - \frac{1}{\eta_2}\dot{\hat{\mathbf{S}}}^T\tilde{\mathbf{S}} - \frac{1}{\eta_3}\dot{\hat{\mathbf{Z}}}^T\tilde{\mathbf{Z}} - \frac{1}{\eta_4}\dot{\hat{\mathbf{R}}}^T\tilde{\mathbf{R}} - \frac{1}{\eta_5}\tilde{\beta}\dot{\hat{\beta}}\end{aligned} \tag{28}$$

Take (20)-(25) into (28), the derivative of V can be rewritten as

$$\begin{aligned}\dot{V}(t) &= -\frac{1}{2}\mathbf{E}^T\mathbf{QE} + \mathbf{E}^T\mathbf{PB}D - \mathbf{E}^T\mathbf{PB}u_C - \frac{1}{\eta_5}(\beta - \hat{\beta})\dot{\hat{\beta}} \\ &\le -\frac{1}{2}\mathbf{E}^T\mathbf{QE} + \mathbf{E}^T\mathbf{PB}D - \hat{\beta}\left|\mathbf{E}^T\mathbf{PB}\right| - (\beta - \hat{\beta})\left|\mathbf{E}^T\mathbf{PB}\right| \\ &\le -\frac{1}{2}\mathbf{E}^T\mathbf{QE} - \left|\mathbf{E}^T\mathbf{PB}\right|(\beta - |D|) \le 0\end{aligned} \tag{29}$$

This implies that $\mathbf{E}(t)$ will converge to zero as $t \to \infty$. As a result the stability of the proposed control system can be guaranteed.

III. EXPERIMENTAL RESULTS

The USM experimental setup is shown in Fig. 3. The TMS320F2812 digital signal processor (DSP) is used for design the proposed control scheme. The USM driver is used to drive the USM, which encoder signal of rotor angle and speed are fed back to the TMS320F2812 to construct closed-loop control.

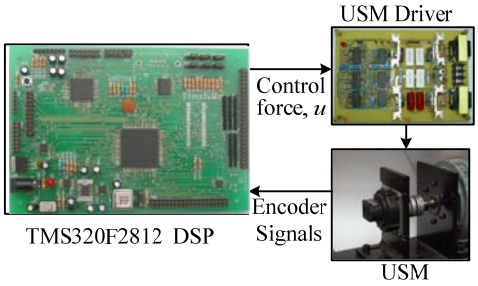

Figure 3. The USM experiment setup.

A. A square angle command from -45 to 45 degree

In Figs. 4, 5 and 6, the USM rotor angle command is a periodic square from -45 to 45 degree. The USM rotor angle and speed responses using the proposed control scheme are depicted in Fig. 4(a). The angle error between the angle command and USM rotor angle is depicted in Fig. 4(b). By observing the experimental result in Fig. 4, the tracking errors can both converge to an acceptable region and the control performance is excellent. The proposed controller retains control performance and has no dead-zone in the construction.

The USM rotor angle and speed responses using the RFNNC without compensated controller are depicted in Fig. 5(a). The angle error is depicted in Fig. 5(b). Compared with the RFNNC without compensated controller in Fig. 5, it can be seen that the RFNNC without compensated controller can achieve barely satisfactory response in each state. But, it exhibits a chattering phenomenon due to the dead-zone especially in slow speed nearby zero.

The USM rotor angle and speed responses using the PI control are depicted in Fig. 6(a). The angle error is depicted in Fig. 6(b). In Fig. 6 illustrated that the PI control has a chattering phenomenon that cannot maintain the control performance when the parameter plant variation is large and the drive conditions change frequently.

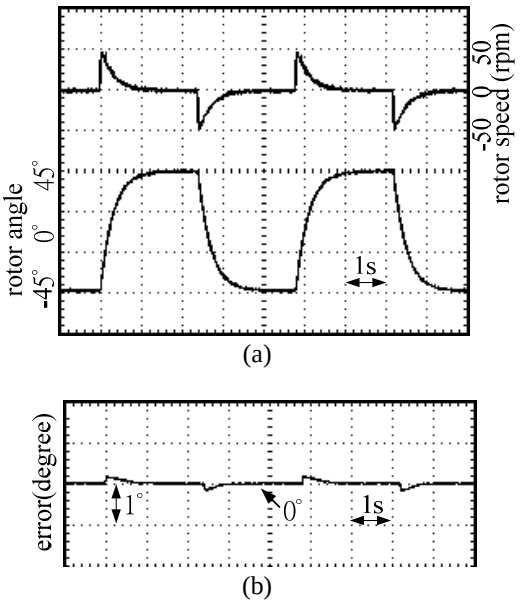

Figure 4. The experimental results using the proposed control scheme for a periodic square command from -45 to 45 degree. (a)USM rotor angle and speed responses, (b) angle error.

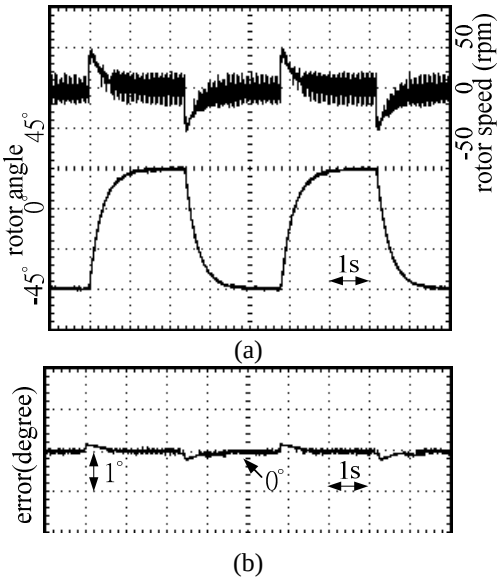

Figure 5. The experimental results using the RFNNC without compensated controller for a periodic square command from -45 to 45 degree. (a) USM rotor angle and speed responses, (b) angle error.

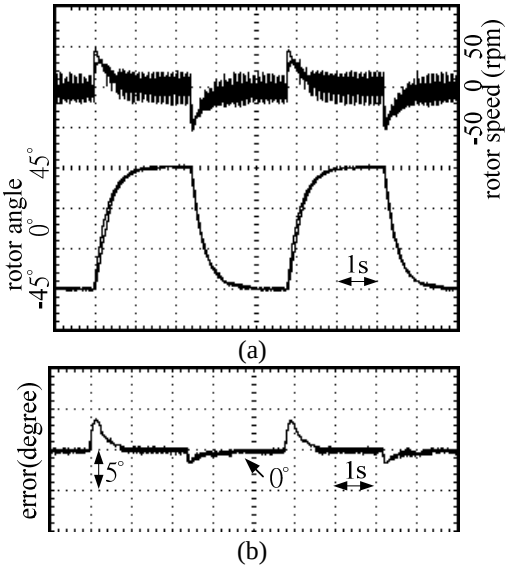

Figure 6. The experimental results using the PI control for a periodic square command from -45 to 45 degree. (a) USM rotor angle and speed responses, (b) angle error.

B. A sinusoidal angle command from -45 to 45 degree

In Figs. 7, 8 and 9 show the USM rotor angle command is a sinusoidal from -45 to 45 degrees. The USM rotor angle and speed responses using the proposed control scheme are depicted in Fig. 7(a). The angle error between angle command and USM rotor angle is depicted in Fig. 7(b). Fig. 7 shows the experimental results with the proposed control scheme that the favorable tracking error is quickly reduced to zero.

 ISBN: 978-1-61208-390-2

The USM rotor angle and speed responses using the RFNNC without compensated controller are depicted in Fig. 8(a). The angle error is depicted in Fig. 8(b). Compared with the RFNNC without compensated controller in Fig. 8, it can be seen that the RFNNC without compensated controller can achieve barely satisfactory response which is similar to the proposed control scheme. However, it exhibits a chattering phenomenon due to the dead-zone especially in slow speed nearby zero.

The USM rotor angle and speed responses using the PI control are depicted in Fig. 9(a). The angle error is depicted in Fig. 9(b). Fig. 9 illustrates that the PI controller tracking response is slower and the steady state error is larger than that of proposed control schemes. The drawbacks of the PI control are interference with the dead-zone and the motor speed has a serious chattering phenomenon at slow speed near zero.

C. A constant speed command of 100 rpm with 0.5 N-m load

Fig. 10 shows the USM rotor speed command is constant at 100 rpm with 0.5N-m load. Fig. 10(a) shows the 0.5N-m load applied to the USM rotor. The USM rotor speed and speed error between the speed command and USM rotor speed using the proposed control scheme are depicted in Fig. 10(b). The USM rotor speed and speed error between the speed command and USM rotor speed using the PI control are depicted in Fig. 10(c). The experimental results in Fig.10 depict that the PI control has larger speed ripple response than the proposed control scheme. Based on the experimental results, the control performance of the proposed control scheme is better than that of PI control.

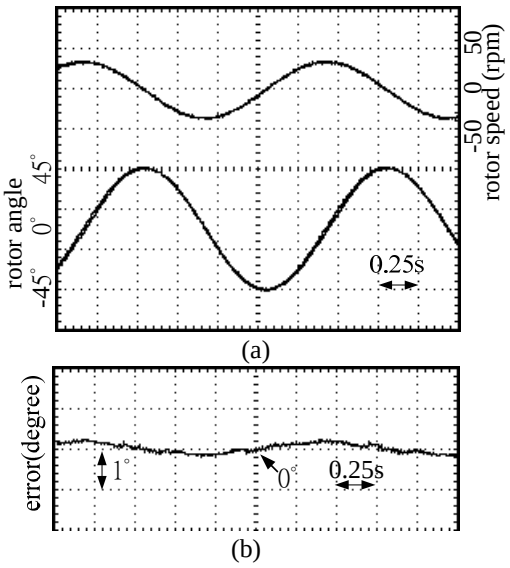

Figure 7. The experimental results using the proposed control scheme for a sinusoidal command from -45 to 45 degree. (a)USM rotor angle and speed responses, (b) angle error.

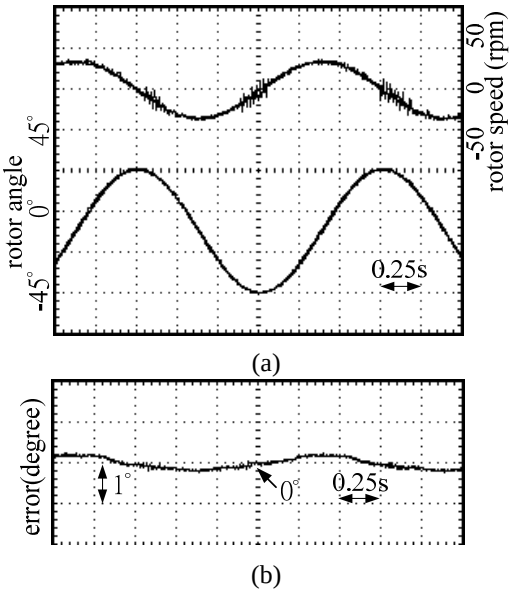

Figure 8. The experimental results using the RFNNC without compensated controller for a sinusoidal command from -45 to 45 degree. (a) USM rotor angle and speed responses, (b) angle error.

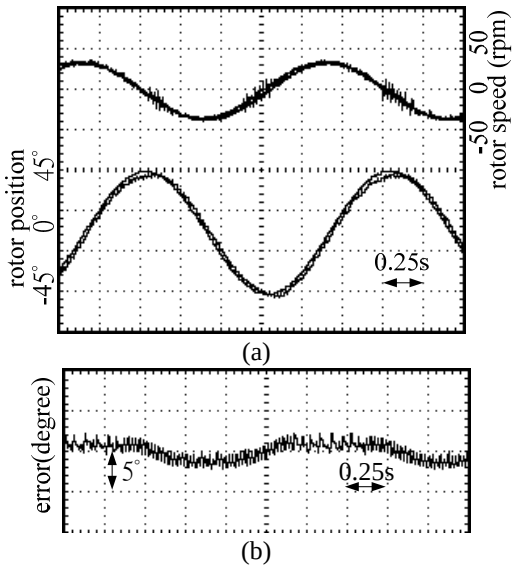

Figure 9. The experimental results using the PI control for a sinusoidal command from -45 to 45 degree. (a) USM rotor angle and speed responses, (b) angle error.

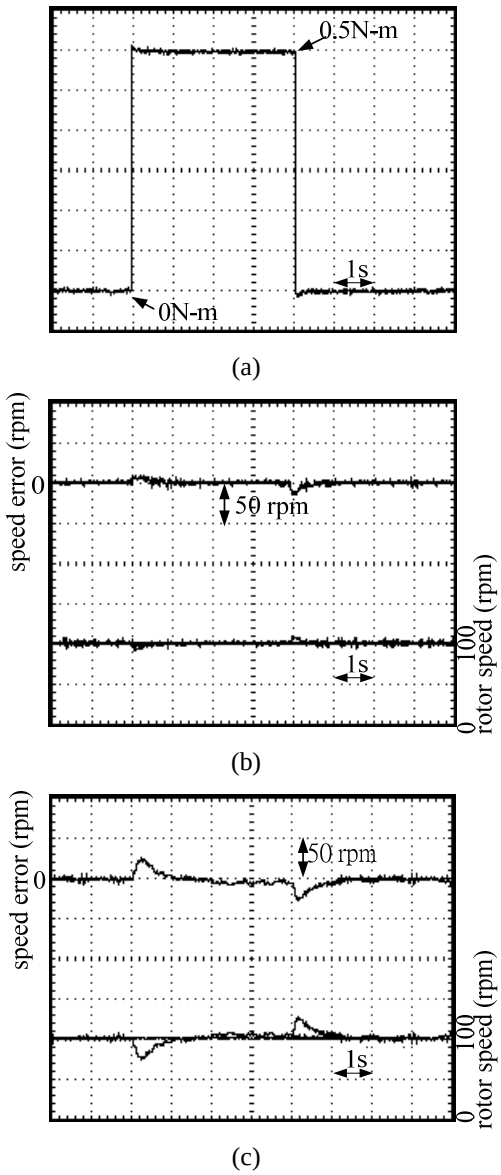

Figure 10. The experimental results for the USM rotor speed command of 100 rpm with 0.5N-m load. (a) applied load, (b) rotor speed and speed error using the proposed control scheme, (c) rotor speed and speed error using the PI control.

IV. CONCLUSIONS

A novel control scheme, using RFNNC combined with a compensated controller, has been applied to USM rotor angle control. The RFNNC is designed in handling nonlinear motor characteristic variations to track the reference angle. A compensated controller is designed to compensate the USM dead-zone effect, which deteriorates the dynamic response. The RFNNC parameters are tuned in the Lyapunov sense; thus, the system stability can be guaranteed. Experimental results show that the proposed control scheme is better than that of PI control.

ACKNOWLEDGMENT

The authors would like to express their appreciation to Ministry of Science Technology for supporting under contact MOST 103-2627-E-168 -001.

REFERENCES

[1] M. A. Tavallaei, Y. Thakur, S. Haider, and M. Drangova," Magnetic-resonance-imaging-compatible remote catheter navigation system," IEEE Trans. Biomedical Engineering, vol. 60, no. 4, pp. 899-905, April 2013.

[2] M. Guo, J. Hu, H. Zhu, C. Zhao, and S. Dong, "Three-degree-of-freedom ultrasonic motor using a 5-mm-diameter piezoelectric ceramic tube," IEEE Trans. Ultrasonics, Ferroelectrics, and Frequency control, vol. 60, no. 7, pp. 1446-1452, July 2013.

[3] H. Y. Wang, K. C. Fan, J. K. Ye, and C. H. Lin, "A long-stroke nanopositioning control system of the coplanar stage," IEEE Trans. Mechatronics, vol. 19, no. 1, pp. 348-356, February 2014.

[4] P. Ci, G. Liu, Z. Chen, S. Zhang, and S. Dong, "High-order face-shear modes of elaxor-PbTiO3 crystals for poezoelectric motor applications," Applied Physics Letters, vol. 104, no. 24, pp. 242911 - 242911-4, July 2014

[5] F. Giraud, P. Sandulescu, M. Amberg, B. Lemaire-Semail, and F. Ionescu, "Modeling and compensation of the internal friction torque of a travelling wave ultrasonic motor," IEEE Trans. Haptics, vol. 4, no. 4, pp. 327-331, 2011.

[6] R. E. Precup, R. C. David, E. M. Petriu, M. B. Radac, and S. Preitl, "Adaptive GSA-based optimal tuning of PI controlled servo systems with reduced process parametric sensitivity, robust stability and controller robustness," IEEE Trans. Cybernetics, vol. 44, no. 11, pp. 1997-2009, November 2013.

[7] T. S. Franklin, J. J. F. Cerqueira, and E. S. de Santana, "Fuzzy and PI controllers in pumping water system using photovoltaic electric generation," IEEE Latin America Transactions, vol. 12, no. 6, pp. 1049-1054, September 2014.

[8] J. Jingzhuo, and B. Liu, "Optimum efficiency control of traveling-wave ultrasonic motor system," IEEE Trans. Industrial Electronics, vol. 58, no. 10, pp. 4822-4829, October 2011.

[9] N. T. Hieu, S. Odomari, T. Yoshida, T. Senjyu, and A. Yona, "Nonlinear adaptive control of ultrasonic motors considering dead-zone," IEEE Trans. Industrial Informatics, vol. 9, no. 4, pp. 1847-1854, November 2013.

[10] S. Zhou and Z. Yao , "Design and optimization of a modal-independent linearultrasonic motor," IEEE Trans. Ultrasonics, Ferroelectrics, and Frequency control, vol. 61, no. 3, pp. 535-546, March 2014.

 ISBN: 978-1-61208-390-2